Stability of Freely Falling Granular Streams

Stephan Ulrich[1] and Annette Zippelius[2,3]

[1]*Instituut-Lorentz for Theoretical Physics, 2333 CA Leiden, Netherlands*
[2]*Institute of Theoretical Physics, Universität Göttingen, 37077 Göttingen, Germany*
[3]*Max-Planck-Institut für Dynamik und Selbstorganisation, 37077 Göttingen, Germany*

(Received 29 February 2012; published 19 October 2012)

A freely falling stream of weakly cohesive granular particles is modeled and analyzed with the help of event driven simulations and continuum hydrodynamics. The former show a breakup of the stream into droplets, whose size is measured as a function of cohesive energy. Extensional flow is an exact solution of the one-dimensional Navier-Stokes equation, corresponding to a strain rate, decaying like t^{-1} from its initial value, $\dot{\gamma}_0$. Expanding around this basic state, we show that the flow is stable for short times, $\dot{\gamma}_0 t \ll 1$, whereas for long times, $\dot{\gamma}_0 t \gg 1$, perturbations of all wavelengths grow. The growth rate of a given wavelength depends on the instant of time when the fluctuation occurs, so that the observable patterns can vary considerably.

DOI: 10.1103/PhysRevLett.109.166001 PACS numbers: 83.50.Jf, 45.70.−n, 47.20.−k

The breakup of a jet of particles is of widespread interest—both for various applications as well as a problem of fundamental interest to physics and applied mathematics. Jets occur on all scales, ranging from the atomic scales of molecular fluids up to the large scale structure of the Universe, e.g., in the context of structure formation in protoplanetary disks. Recently several groups have done experiments on granular streams, revealing many features which are familiar from molecular liquids—even though the constituents, the grains, are macroscopic objects.

While hard spheres with a very short ranged attractive potential are shown to phase separate into a solid and infinitely dilute gas [1], a somewhat surprising observation was the clustering [2–4] in freely falling *dry* granular streams which are reminiscent of the droplet patterns observed in liquids due to surface tension. Even though tiny attractive forces could be measured and are attributed to van der Waals interactions or capillary bridges, the observed size of the clusters did not agree with the predictions of Rayleigh and Plateau. In another set of experiments [5,6], capillary waves and their dispersion were measured, allowing them to deduce a (tiny) surface tension. Exciting perturbations of a given frequency and observing their initial growth was consistent with the Rayleigh-Plateau analysis.

In this Letter, we model a freely expanding stream of weakly cohesive, inelastically colliding grains and simulate it for the parameters deduced from experiment. We confirm the observed clustering and determine growth rates and drop sizes in dependence on cohesive energy. The initial instability is analyzed within a continuum description, based on the Navier-Stokes equations. Given an exact solution of the nonlinear equations for extensional flow, linear stability analysis can be performed and predicts nonmonotonic behavior as a function of time: For short times a finite strain rate stabilizes the stream, whereas for long times it becomes completely unstable.

Cohesive forces—We model [7] the grains as hard spheres of diameter d. When two particles approach they do not interact until they are in contact whereupon they are inelastically reflected with a coefficient of restitution ε. Moving apart, the particles feel an attractive potential of range $d_{\mathrm{cf}} = 0.01d$. Such an attractive force can be due to capillary bridges or van der Waals forces, if the particles are deformed in collisions. As the spheres withdraw beyond the distance d_{cf}, a constant amount of energy W_{coh} is lost provided the normal relative velocity Δv of the impacting particles is sufficient to overcome the potential barrier, $\Delta v > \Delta v_{\mathrm{crit}} = \sqrt{2W_{\mathrm{coh}}/\mu}$ (where μ is the reduced mass); otherwise the particles form a bounded state, oscillating back and forth.

Strain rate—We assume that the particles fall out of the container into a vacuum [8] with an initial velocity v_0. For simplicity, consider a column of n particles leaving the hopper sequentially, with a time interval $\Delta t = d/v_0$, and ignore collisions for now. Leaving the hopper at $t = i\Delta t$, the ith particle will be accelerated due to the gravitational acceleration g, implying $z_i(t) = \frac{1}{2}g \cdot (t - i\Delta t)^2 + v_0 \cdot (t - i\Delta t)$. (The initial conditions are $\dot{z}_i(i\Delta t) = v_0$ and $z_i(i\Delta t) = 0$.) Hence the resulting stream has a *velocity gradient*, which can be computed from

$$\frac{dv}{dz} = \frac{\dot{z}_{i-1}(t) - \dot{z}_i(t)}{z_{i-1}(t) - z_i(t)} = \frac{g\Delta t}{gt\Delta t + v_0\Delta t} = \frac{\dot{\gamma}_0}{1 + \dot{\gamma}_0 t}. \quad (1)$$

Here $\dot{\gamma}_0 = g/v_0$ is the *initial* strain rate and we have ignored terms of $\mathcal{O}(\Delta t)^2$. The *time dependent* strain rate is essential for the stability analysis: stretching is known [9] to stabilize the flow and hence prevent clustering. As we will see below, this is precisely what happens for short times, whereas for long times we recover the clustering

instability, when the strain rate has become sufficiently small.

Simulation—This simple model can be simulated with an event driven code [7], allowing us to consider large systems with up to $N = 10^6$ particles. We simulate the freely falling stream in the rest frame of the stream: Initially all particles are contained in a cylindrical volume, whose centre of mass is at rest during all of the simulation, mimicking the experimental setup, where the camera moves with the falling stream [3]. In the initial state, we impose a homogeneous velocity gradient $\dot{\gamma}_0 = \frac{dv}{dz} = \frac{g}{v_0}$ together with a small random velocity [10]. Given the instantaneous interactions in our simple model, the strain rate $\dot{\gamma}_0$ and the cohesive energy W_{coh} are not independent parameters: If, e.g., $\dot{\gamma}_0$ is increased by a factor of two and W_{coh} by a factor of 4, the particles follow exactly the same trajectories, just twice as fast. Hence, we only vary the cohesive energy, $w := W_{\mathrm{coh}}/W_{\mathrm{coh,exp}}$, which is conveniently measured relative to the typical experimental value of Ref. [3], i.e., $W_{\mathrm{coh,exp}} = 10^{-15}$ J. The cohesive energy relates to the surface tension, used later, through $\gamma = W_{\mathrm{coh}}/d^2$ [3,11]. The remaining parameters are chosen, unless specified otherwise, to match the typical experimental values, namely the coefficient of restitution $\varepsilon = 0.9$, the stream's initial volume fraction $\phi = 0.5$, the initial strain rate $\dot{\gamma}_0 = 98.1\ \mathrm{s}^{-1}$, and the initial stream radius $r_0 = 19d$.

Simulation results—Figure 1 shows snapshots of the same system at five different times, demonstrating, how the initially straight stream profile develops inhomogeneities, which grow in time and finally lead to separate clusters. In the Supplemental Material, we furthermore confirm that the droplet formation is indeed attributed to the cohesive interactions [12] and not to other mechanisms inherent of granular fluids.

In the inset of Fig. 2, we plot the mean droplet size N_{drop} as a function of time for two values of W_{coh}. After a sharp initial decrease due to separation of the stream into clusters, N_{drop} reaches a steady state. Its value is shown in the main plot for a range of cohesive energies. Scaling arguments in Ref. [4] suggest that the typical length of a droplet, rescaled back to its length on the unstretched stream, λ_0, should scale like the square root of the cohesive energy. Hence, we expect $N_{\mathrm{drop}} \propto \lambda_0 \propto W_{\mathrm{coh}}^{1/2}$. The solid line is a fit to the data points with an exponent $\beta = 0.54$, confirming the simple scaling arguments.

The actual shape of the droplet is more difficult to capture systematically than its mass, since it continues to change slightly even after the droplets have separated. Royer *et al.* [3] characterize droplets by their length λ_c and width w_c, right before they hit the bottom of the experimental setup. They find that droplets' aspect ratios λ_c/w_c always fall in between 1 and 3. Even though the droplet formation appears to be surface tension driven, these findings preclude the expected Rayleigh-Plateau instability as a predominant mechanism (which only allows aspect ratios $\geq \pi$). In Fig. 3, we show the simulation results for the droplet lengths and width for various W_{coh}. The most striking feature in this plot is the huge scatter in droplet length for a given value of W_{coh}. This result is at variance with a well defined critical wavelength, corresponding to the fastest growing mode.

Previous findings suggest that droplet formation is due to an instability, causing small fluctuations at certain wavelengths to grow, while other wavelengths are stable. To shed light on this instability, we impose a small amplitude variation of stream radius, $h(z) = r_0 + A\cos(kz)$, in the initial state. The cylindrical symmetry is preserved and the volume is kept constant. We follow the time evolution of

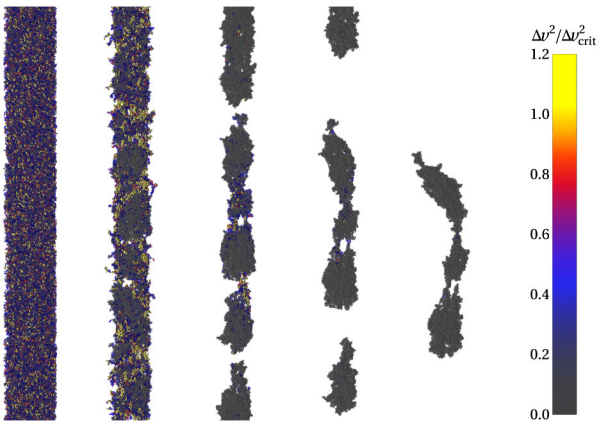

FIG. 1 (color online). Snapshots of the system for different times; colors (gray scales) indicate relative velocities Δv of cohesively interacting particles; small droplets of size $N_{\mathrm{drop}} < 100$ are ignored for better visibility. See Ref. [19] for a movie.

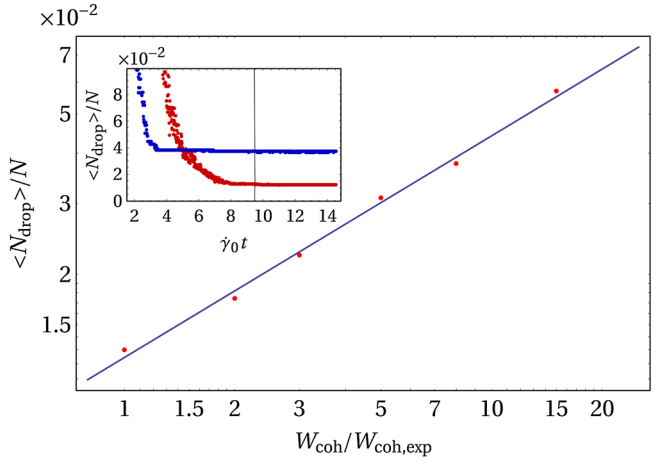

FIG. 2 (color online). Mean droplet size $\langle N_{\mathrm{drop}} \rangle$ as a function of $w = W_{\mathrm{coh}}/W_{\mathrm{coh,exp}}$; data points are results from the simulation and the solid line is a power law fit; inset: mean droplet size $\langle N_{\mathrm{drop}} \rangle$ as a function of time for $w = 8$ (high final value) and $w = 1$ (low final value); at the grey vertical line all systems have reached a steady state, which is used for the main plot.

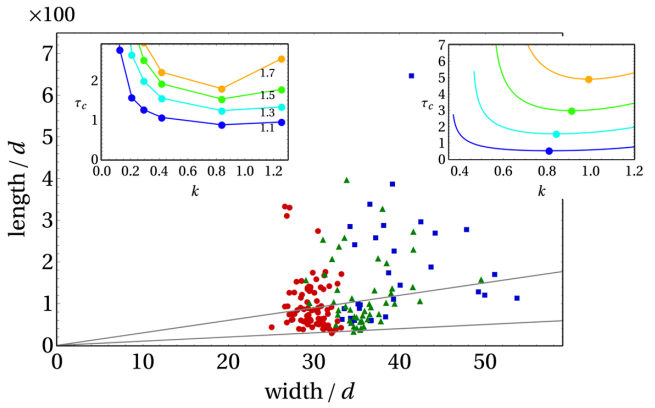

FIG. 3 (color online). Length vs width of individual clusters with $N_{\mathrm{drop}} \geq 1000$; $w = 1$ (disk), $w = 3$ (triangle), and $w = 8$ (square); gray lines correspond to aspect ratios of 1 and 3; insets: time $\tau_c = \dot{\gamma}_0 t_c$ for an imposed perturbation of wave number k (in units of particle diameter d) to grow beyond a given value A_c (1.7, 1.5, 1.3, 1.1 from top to bottom); left inset: simulation with $r_0 = 10d$; right inset: analytical theory

the respective Fourier mode $A(k, t)$ and determine the time t_c, it takes the amplitude to grow beyond a certain value A_c, i.e., $A(k, t_c)/A(k, 0) = A_c$. This result is shown in the left inset of Fig. 3. A fastest growing mode can be identified and hardly depends on the choice of A_c. In the following section, we study this instability in terms of a continuum theory and compare the predictions to simulation and experiment.

Continuum theory—To analyze the stability of the initially homogeneous stream we use continuum theory [9,13]. Our starting points are the Navier-Stokes equations for the velocity field, $\vec{v}(r, z; t)$, in cylindrical coordinates assuming axial symmetry

$$\partial_t \vec{v} + (\vec{v} \cdot \nabla)\vec{v} = -\frac{\nabla p}{\rho} + \nu \Delta \vec{v}, \tag{2}$$

together with the equation of motion for the interface $r = h(z, t)$,

$$\partial_t h + v_z \partial_z h = v_r|_{r=h}. \tag{3}$$

Here p denotes the pressure, ρ the density, and ν the shear viscosity. These equations have to be solved, subject to the boundary conditions, requiring the balance of normal and tangential forces at the interface: $\sigma_{ij} n_j = -\kappa \Gamma \rho n_i$ at $r = h$. Here κ is the curvature of the interface (see Ref. [14] for its dependence on h), $\Gamma = \gamma/\rho$ is the surface tension divided by the density and $\sigma_{ij} = -p\delta_{ij} + \nu(\partial_i v_j + \partial_j v_i)\rho$ denotes the stress tensor.

To obtain approximate solutions to the above equations, we follow Eggers [9] and assume that variations in the radial direction take place on small scales compared to variations along the stream. Under these assumptions, a one dimensional Navier-Stokes equation for $v = v_z(z, t)$ has been derived [9] for an incompressible fluid:

$$\partial_t v + v v' = -\Gamma \kappa' + 3\nu \frac{(v' h^2)'}{h^2} \tag{4}$$

$$\partial_t h^2 + (v h^2)' = 0, \tag{5}$$

where prime refers to a derivative with respect to z.

These equations have been studied in various circumstances for molecular fluids [9,13]. The best known one is the Rayleigh Plateau instability, where one expands around a state with constant radius and velocity which does not apply in the presence of gravity. Jet flow dominated by viscous effects [15,16] has also been analyzed within the above one-dimensional model. Here we consider instead a freely falling stream [17] in the comoving frame. This state is characterized by a time dependent velocity gradient, that is constant in space: $\bar{v}(z, t) = \frac{z\dot{\gamma}_0}{1+\dot{\gamma}_0 t}$. Incompressibility requires $\bar{h}(z, t) = r_0(1 + \dot{\gamma}_0 t)^{-1/2}$. These fields solve the above equations *exactly*, allowing us to do a linear stability analysis by expanding around the above solution.

We introduce a dimensionless position variable $Z := z/[r_0(1 + \dot{\gamma}_0 t)]$ such that Z remains fixed, if z moves along with the stream. The Z dependence can then be taken care of by plane waves: $\sim \exp(ikr_0 Z)$. To further simplify the notation, we introduce dimensionless time $\tau = \dot{\gamma}_0 t$ and wave number $K = kr_0$. We obtain two linear equations for $h(z, t) - \bar{h}(z, t) = \exp(iKZ)\epsilon_R(\dot{\gamma}_0 t)$ and $v(z, t) - \bar{v}(z, t) = \exp(iKZ)\dot{\gamma}_0 \epsilon_V(\dot{\gamma}_0 t)$:

$$\begin{aligned} \dot{\epsilon}_V(\tau) &= -\frac{\epsilon_V(\tau)}{1+\tau} + iK\left(\tilde{\Gamma} - \frac{\tilde{\Gamma} K^2}{(1+\tau)^3}\right)\epsilon_R(\tau), \\ \dot{\epsilon}_R(\tau) &= -\frac{\epsilon_R(\tau)}{2(1+\tau)} - \frac{iK\epsilon_V(\tau)}{2(1+\tau)^{3/2}}. \end{aligned} \tag{6}$$

For clarity of presentation we have set $\nu = 0$ and hence are left with one dimensionless parameter $\tilde{\Gamma} = \Gamma/(r_0^3 \dot{\gamma}_0^2)$. The generalization to finite viscosity is straightforward and given in the Supplemental Material [14].

The above equations are two ordinary differential equations with *time-dependent* coefficients. This makes the stability analysis complex, because a given wave number, which is stable at t_0, can override an initially unstable mode in the course of time. Of course the equations can easily be integrated numerically. Before discussing the generalized eigenvalue problem, we try to extract the qualitative behavior by inspecting the equations for small and large times. For $\tau = \dot{\gamma}_0 t \lesssim 1$ we expect the initial strain rate to have a stabilizing effect, in particular for long wavelength perturbations. For long times, $\tau = \dot{\gamma}_0 t \gtrsim 1$, on the other hand, the strain rate decays. With the ansatz $\epsilon_V, \epsilon_H \sim e^{\lambda \tau}$ one finds for $\tau \gg 1$

$$\lambda_\pm = -\frac{3}{4(1+\tau)} \pm \left(\frac{\tilde{\Gamma} K^2}{2(1+\tau)^{3/2}} + \frac{1}{16(1+\tau)^2}\right)^{1/2},$$

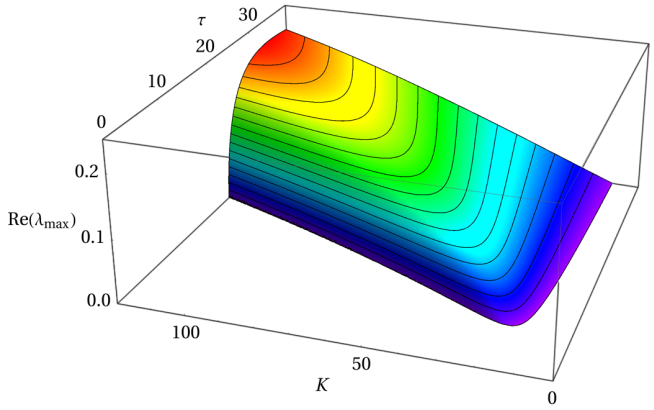

FIG. 4 (color online). Real part of the unstable eigenvalue as a function of wave number and time. $\tilde{\Gamma}$ has the experimental value $\tilde{\Gamma}_{\mathrm{exp}}$ and $\nu = 0$.

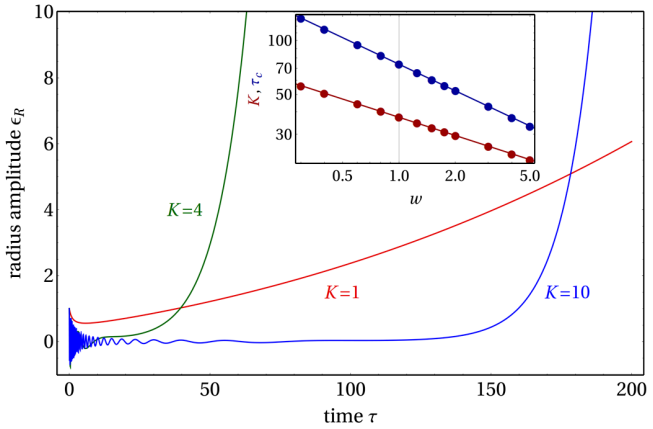

FIG. 5 (color online). Example for growth of perturbations, obtained from integrating the linearized equations; inset: most unstable wave number and time of growth to increase by 50% in dependence on $w = \Gamma/\Gamma_{\mathrm{exp}}$.

that *all wave numbers are unstable* for sufficiently large τ, because the dominant term is the one involving the surface tension ($\tilde{\Gamma}$). To discuss the general case, we compute the eigenvalues for all K and t, by diagonalizing the time-dependent matrix of coefficients. The larger eigenvalue, λ_{max},—responsible for the instability—is shown in Fig. 4 as a function of K and t in the range of values, where $\lambda_{\mathrm{max}} > 0$. The parameters for the initial strain rate, $\dot{\gamma}_0$, and the surface tension, Γ, are taken from experiment and the viscosity is set to zero. We observe that initially all wavelengths are stable for $t = 0$, the first instability sets in at $\tau \approx 8$ and $K \approx 15$. Note that (i) the wave numbers K are the initially imposed ones and have to be scaled down by the stretching factor $1 + \tau$, when the stream has been stretched up to time τ, and (ii) that wave numbers are measured in units of the *initial* radius of the stream, whereas the actual radius decreases according to $r(\tau) = r_0/(1 + \tau)^{1/2}$. Hence to obtain the ratio of wavelength to radius at time τ, when the instability occurs, we have to scale wave numbers according to $\tilde{K}(\tau) = K(1 + \tau)^{-3/2}$. If one plots the eigenvalue versus $\tilde{K}(\tau)$, one observes a ridge [14] at approximately $\tilde{K} \approx 1$, implying that at each instant of time τ—while the stream is stretching—unstable modes with roughly the wavelength of Rayleigh Plateau are growing.

However, we stress that our system is not in a stationary state, but expanding. As a consequence the eigenvalues are time dependent, and whether a perturbation increases or decreases depends on the time of its occurrence. In Fig. 5, we show an example of the integrated Eq. (6) with 3 modes excited initially ($\epsilon_R = 1$ for $K = 1, 4, 10$). As expected from the eigenvalue analysis, initially all modes are stable, then the smallest K starts to grow, but is—at later times—overridden by the larger wave numbers. This is meant to illustrate that the observed pattern will depend on the instant, when a fluctuation with a particular wave number occurs.

For a quantitative comparison with simulations we numerically integrate Eq. (6) to determine the time $\tau_c(K)$, which it takes an initial perturbation to grow by a factor A_c. The result is shown in the right inset of Fig. 3 for a value of the reduced viscosity $\nu/(r_0^3\dot{\gamma}_0^2) = 0.2$ and should be compared to the left inset of Fig. 3. The "dispersion relation" for $A_c = 1.1$ agrees well. The perturbations grow faster in the simulation than predicted by continuum theory, which is presumably due to the limited validity of the linear theory.

Variation of the parameters—If the viscosity is increased and/or the coefficient of restitution set to one, the results remain qualitatively the same (see Supplemental Material [14,18] for details). If the initial strain rate is put to zero, we recover the Rayleigh-Plateau instability. Interesting effects are observed by varying the cohesive energy. Decreasing the cohesive energy, $\Gamma < \Gamma_{\mathrm{exp}}$, the initial range of unstable wave numbers shifts to larger K, i.e., smaller wavelength, in agreement with simulations (see Fig. 2). We determine the time $\tau(K)$ which it takes an unstable mode of wave number K to grow by 50% from its initial value for several values of cohesive energy. In that way we can deduce the critical wave number and the time for the stability to occur as a function of Γ. These are shown in the inset of Fig. 5. We clearly observe an increase in critical wavelength with Γ in agreement with simulation and experiment. Furthermore for increased Γ the instability occurs earlier.

Conclusions—We have shown that a stream of granular particles falling under gravity is generically unstable due to surface tension—even though the Rayleigh-Plateau argument does not apply. In the comoving frame, the stream is freely expanding, implying that the initially straight profile is subject to a time-dependent strain rate. Linearizing the Navier-Stokes equation around this nonstationary state, we have shown that the strain rate stabilizes the straight

flow profile at short times, whereas for long times all wave numbers are unstable. Since we expand around a nonstationary state, the growth rate of a given wavelength depends on the time, when the corresponding fluctuation occurs spontaneously or is introduced into the flow. Thus, a variety of patterns may be observed including behavior reminiscent of the Rayleigh-Plateau instability [6].

We are grateful to Heinrich Jaeger for suggesting applying a model of cohesive particles to freely falling streams. Furthermore we acknowledge interesting discussions with him and Scott Waitukaitis.

[1] R. P. Sear, Phys. Rev. E **59**, 6838 (1999).
[2] M. E. Möbius, Phys. Rev. E **74**, 051304 (2006).
[3] J. R. Royer, D. J. Evans, L. Oyarte, E. Kapit, M. Möbius, S. R. Waitukatis, and H. M. Jaeger, Nature (London) **459**, 1110 (2009).
[4] S. R. Waitukaitis, H. F. Grütjen, J. R. Royer, and H. M. Jaeger, Phys. Rev. E **83**, 051302 (2011).
[5] Y. Amarouchene, J.-F. Boudet, and H. Kellay, Phys. Rev. Lett. **100**, 218001 (2008).
[6] G. Prado, Y. Amarouchene, and H. Kellay, Phys. Rev. Lett. **106**, 198001 (2011).
[7] S. Ulrich, T. Aspelmeier, K. Roeller, A. Fingerle, S. Herminghaus, and A. Zippelius, Phys. Rev. Lett. **102**, 148002 (2009); S. Ulrich, T. Aspelmeier, A. Zippelius, K. Roeller, A. Fingerle, and S. Herminghaus, Phys. Rev. E **80**, 031306 (2009).
[8] This is in contrast to [A. Alvarez, E. Clement, and R. Soto, Phys. Fluids **18**, 083301 (2006)], who inject the particles into a suspension.
[9] J. Eggers, Rev. Mod. Phys. **69**, 865 (1997).
[10] A Maxwell distributed random velocity is added to each particle. Its temperature has to be well below W_{coh} to allow phase separation into droplets and a dilute gas.
[11] J. S. Rowlinson and B. Widom, *Molecular Theory of Capillarity* (Clarendon, Oxford, 1982)
[12] See Supplemental Material at http://link.aps.org/supplemental/10.1103/PhysRevLett.109.166001 for a movie of a granular stream $\varepsilon = 0.9$ *without* adhesion $W_{\mathrm{coh}} = 0$.
[13] J. Eggers and E. Villermeaux, Rep. Prog. Phys. **71**, 036601 (2008).
[14] See Supplemental Material at http://link.aps.org/supplemental/10.1103/PhysRevLett.109.166001 for the generalization of (6) as well as its further analysis and implications.
[15] U. S. Sauter and H. W. Buggisch, J. Fluid Mech. **533**, 237 (2005).
[16] S. Senchenko and T. Bohr, Phys. Rev. E **71**, 056301 (2005).
[17] I. Frankel and D. Weihs, J. Fluid Mech. **155**, 289 (1985).
[18] See Supplemental Material at http://link.aps.org/supplemental/10.1103/PhysRevLett.109.166001 for a movie, showing that droplet formation also persists for $\varepsilon = 1$. ($W_{\mathrm{coh}} = 8W_{\mathrm{coh,exp}}$).
[19] See Supplemental Material at http://link.aps.org/supplemental/10.1103/PhysRevLett.109.166001 for a movie showing the stream's evolution and droplet formation.